JGR Oceans

RESEARCH ARTICLE
10.1029/2020JC016535

Key Points:

- A rapid erosion of bottom water thermohaline signatures was observed off Minorca Island during the Western Mediterranean Transition's (WMT) initial stages
- Local evolution of the WMT deep hydrographic structure during 2005–2007 is consistent with persistent intense mixing
- Evidence that intense mixing occurs at the continental slope and mixed waters are exported offshore is found

Supporting Information:

- Supporting Information S1
- Movie S1

Correspondence to:
S. Piñeiro,
safo.pineiro@ieo.es

Citation:
Piñeiro, S., González-Pola, C., Fernández-Díaz, J. M., Naveira-Garabato, A. C., Sánchez-Leal, R., Puig, P., et al. (2021). Persistent, depth-intensified mixing during the Western Mediterranean Transition's initial stages. *Journal of Geophysical Research: Oceans*, *126*, e2020JC016535. https://doi.org/10.1029/2020JC016535

Received 21 JUN 2020
Accepted 5 DEC 2020

Persistent, Depth-Intensified Mixing During The Western Mediterranean Transition's Initial Stages

S. Piñeiro[1], C. González-Pola[2], J. M. Fernández-Díaz[3], A. C. Naveira-Garabato[4], R. Sánchez-Leal[5], P. Puig[6], J. Salat[6], and R. Balbin[1]

[1]Centro Oceanográfico de Baleares, Instituto Español de Oceanografía, Palma, Spain, [2]Centro Oceanográfico de Gijón, Instituto Español de Oceanografía, Gijón, Spain, [3]Department of Physics, Universidad de Oviedo, Oviedo, Spain, [4]University of Southampton, National Oceanography Centre, Ocean and Earth Science, Southampton, UK, [5]Centro Oceanográfico de Cádiz, Instituto Español de Oceanografía, Cádiz, Spain, [6]Institut de Ciències del Mar, Consejo Superior de Investigaciones Científicas, Barcelona, Spain

Abstract

Major deep-convection activity in the northwestern Mediterranean during winter 2005 triggered the formation of a complex anomalous deep-water structure that substantially modified the properties of the Western Mediterranean deep layers. Since then, evolution of this thermohaline structure, the so-called Western Mediterranean Transition (WMT), has been traced through a regularly sampled hydrographic deep station located on the outer continental slope of Minorca Island. A rapid erosion of the WMT's near-bottom thermohaline signal was observed during 2005–2007. The plausible interpretation of this as local bottom-intensified mixing motivates this study. Here, the evolution of the WMT structure through 2005–2007 is reproduced by means of a one-dimensional diffusion model including double-diffusive mixing that allows vertical variation of the background mixing coefficient and includes a source term to represent the lateral advection of deep-water injections from the convection area. Using an optimization algorithm, a best guess for the depth-dependent background mixing coefficient is obtained for the study period. WMT evolution during its initial stages is satisfactorily reproduced using this simple conceptual model, indicating that strong depth-intensified mixing ($K^{vc}(z) \approx 22 \times 10^{-4}$ m^2 s^{-1}; $z \gtrapprox$ 1,400 dbar) is a valid explanation for the observations. Extensive hydrographic and current observations gathered over the continental slope of Minorca during winter 2018, the first deep-convective winter intensively sampled in the region, provide evidence of topographically localized enhanced mixing concurrent with newly formed dense waters flowing along-slope toward the Algerian sub-basin. This transport-related boundary mixing mechanism is suggested to be a plausible source of the water-mass transformations observed during the initial stages of the WMT off Minorca.

Plain Language Summary

In winter 2005, an exceptional production of deep waters with anomalous temperature and salinity induced a series of drastic changes in the deep waters of the Western Mediterranean. The evolution of these new deep waters was traced up to the present day through hydrographic measurements in the outer continental slope of Minorca. During 2005–2007, a rapid erosion of the bottom water characteristics was observed. This may be indicative of enhanced mixing near the seafloor. By means of an idealized numerical model, the evolution of the deep waters off Minorca during that period is satisfactorily reproduced, indicating that the deep waters experienced persistent, strongly depth-intensified mixing. More than a decade later, extensive hydrographic and current observations gathered above the continental slope of Minorca evidence enhanced bottom mixing associated with the along-slope flow of newly formed deep waters during winter of 2018, a much less relevant winter in terms of deep-water formation albeit intensively sampled. This boundary mixing mechanism is suggested to be a plausible source of the strong mixing necessary to reproduce the observed evolution of the deep waters during the 2005–2007 period, as indicated by our modeling approach.

1. Introduction

The Gulf of Lion (GoL) is well known to be an active dense-water formation area (Figure 1a; MEDOC Group, 1970). In this region, the Western Mediterranean Deep Water (WMDW) is formed in winter in some years by open-ocean deep convection (Marshall & Schott, 1999), with additional, intermittent contributions

of distinct dense waters formed over the continental shelf that cascade along the continental slope and submarine canyons (Canals et al., 2006; Durrieu De Madron et al., 2005).

During winter 2005, an extraordinary deep convection event injected large amounts of heat and salt into the deep Western Mediterranean (WMED), initiating a new stage in the historical evolution of its thermohaline characteristics (Font et al., 2007; López-Jurado et al., 2005; Schroeder et al., 2006). This shift, termed Western Mediterranean Transition (WMT; Font et al., 2009; Schroeder et al., 2016), modified the stratification of the deep layers through the occurrence of a complex deep-water structure with a distinctive hook-shaped signature in the θ–S plane. Such a signature was formed via contributions of two distinct water masses: a warmer and saltier deep water (nWMDW) formed in the open ocean and located beneath the old WMDW (oWMDW), and a cascading-origin colder and fresher dense water mass at the bottom (cWMDW) (see notations in Figure 2; Salat et al., 2006).

Since then, the original WMT signal has been eroded by diffusive mixing and subsequent instances of deep-water renewal, resulting in a denser, warmer, saltier, and more stratified deep water (relative to that present before 2005) that currently (as of 2020) fills the deepest layers of the WMED. The long-term thermohaline evolution of the deep layers during the WMT was tracked by means of a seasonally occupied deep hydrographic station located in the outer continental slope of Minorca Island (Figure 1), analyzed in detail by Piñeiro et al. (2019). This comprehensive dataset enabled the study of deep-ocean mixing dynamics and their impact on the large-scale thermohaline evolution of the regional water masses. A remarkable feature of the WMT hydrographic structure evolution shown by Piñeiro et al. (2019) was the rapid erosion of the cWMDW-nWMDW portion of the water column during 2005–2007, concurrent with a prominent increase in the θ–S maximum associated with the nWMDW core (Figure 2).

During the winter of 2006 (the following winter after the WMT onset), the deep-water formation area of the WMED was extended to the Ligurian Sea (Smith et al., 2008), and anomalous dense waters were formed again (Schroeder et al., 2008) with a much less relevant contribution of cascading waters (Fuda et al., 2009; Puig et al., 2013; Schroeder et al., 2013). No deep convection was reported in the two following winters (2007–2008; Houpert et al., 2016; Puig et al., 2013; Schroeder et al., 2013; Somot et al., 2018). The observed rapid erosion of the cWMDW-nWMDW water column structure during 2005–2007 may thus be indicative of enhanced near-bottom mixing.

Our goal in this work is to establish whether the observed evolution of the WMT hydrographic structure during 2005–2007 is indeed consistent with increased mixing near the seafloor, combined with the advection of warmer and saltier waters at shallower levels. To evaluate this hypothesis, we set up a one-dimensional diffusion model including double-diffusive mixing schemes that incorporates (i) a source term to represent the lateral advection of newly formed dense waters under simple and realistic assumptions, and (ii) a depth-dependent vertical mixing coefficient that can be tuned so the simulated evolution of hydrographic structure may resemble the overall observed evolution.

The outcomes of our analysis are discussed by reference to the local changes in density structure and circulation measured during a much less dramatic, albeit intensively sampled, deep convective period in winter 2018. Since no extensive regional observations during the WMT initial stages are available, these measurements enable us to explore the impinging of newly formed deep waters on the continental slope of Minorca and deep-ocean mixing dynamics during post-convective periods. The dataset entails two high-resolution Conductivity-Temperature-Depth (CTD) sections in the NE flank of the continental slope of Minorca occupied in 2017–2018, and a three current meter mooring deployed in the outer part of the slope during 2015–2018.

The paper is organized as follows. Data sets used in this study, the 2005–2007 observations and the working hypotheses are presented in Section 2. Section 3 describes the one-dimensional diffusion model setup, the spatio-temporal configuration of the advective term, and the mixing coefficient profile optimization procedure. Section 4 explicitly presents the configuration of the experiments. In Section 5, results are reported, to be subsequently discussed in Section 6. Final considerations and conclusions are gathered in Section 7.

2. Observational Record and Initial Hypotheses

2.1. The Minorca Time Series

The Minorca deep station (40°10.00′ N, 04°34.96′ E, 2,540 m deep; red vertical line in Figure 1b) is one of the deep hydrographic stations located along the Mediterranean continental slope of the Iberian Peninsula that are seasonally occupied by the RADMED monitoring program (*'RADiales del MEDiterráneo';* López-Jurado et al., 2015) and other supporting projects. It is located to the NE of Minorca Island on the outer continental slope, within the main advective pathway of the newly formed dense waters from the GoL toward the Algerian sub-basin (Beuvier et al., 2012; Durrieu de Madron et al., 2013). This station was first sampled in 2001, and established in 2005 as a deep-water observatory to track the evolution of the WMED hydrographic structure following the WMT. After 15 years of monitoring and 45 seasonal occupations (2005–2020), the station offers a detailed picture of the variability in WMED deep layers induced by this climatic event and successive injections of dense waters up to the present. All CTD casts in this time series were obtained, processed and calibrated following common oceanographic standards (RADMED program protocols as described in López-Jurado et al., 2015).

Since this study focuses on the thermohaline evolution of the deep waters observed off Minorca during the 2005–2007 period, we consider as our observational record for the study period a subset (July 15, 2005–January 6, 2007) of the fortnightly hydrographic time series used in Piñeiro et al. (2019). These time series were constructed by spatio-temporally smoothing of the raw profiles of the Minorca deep station during

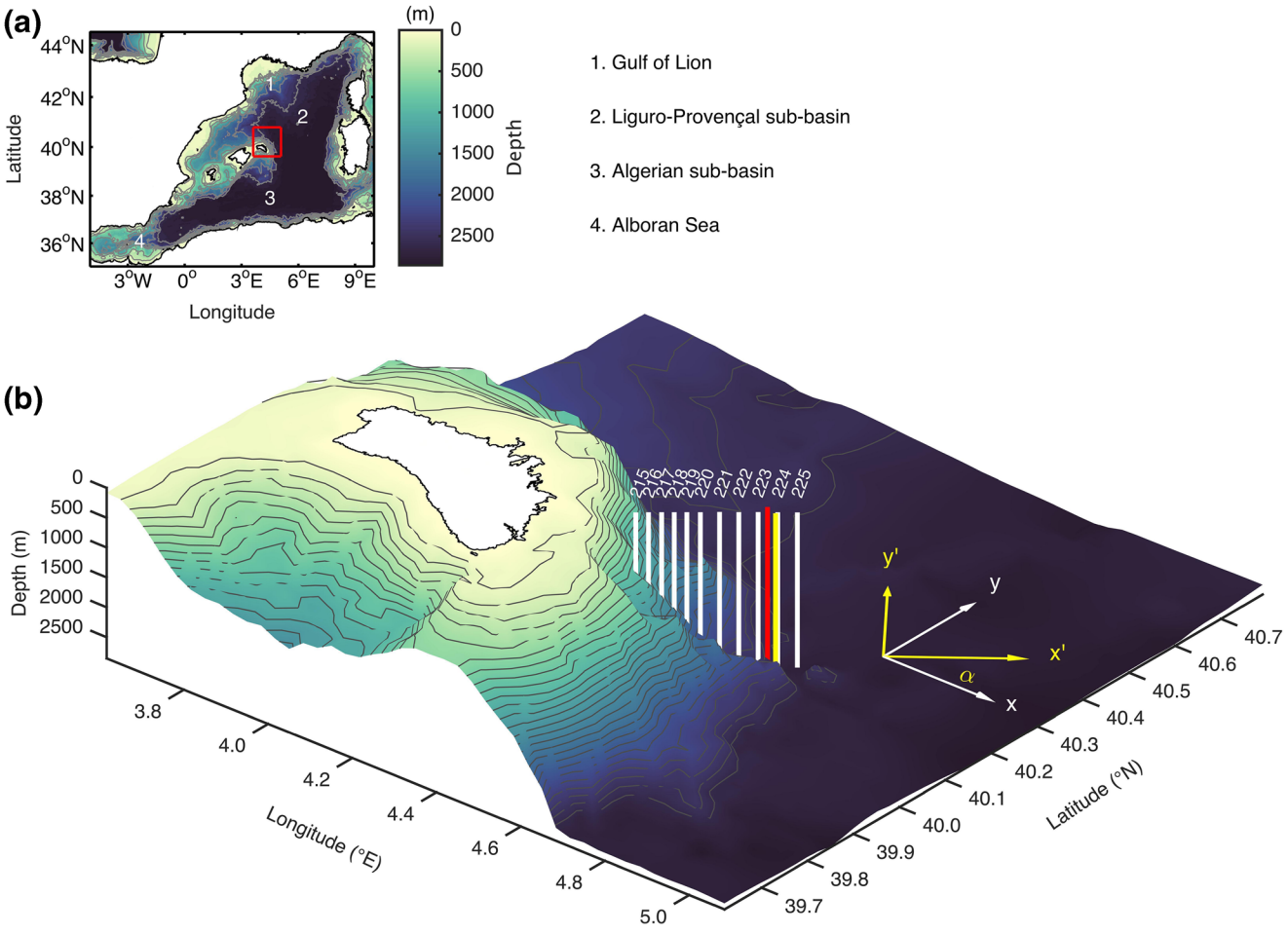

Figure 1. (a) Location of the study area (red square). (b) Three-dimensional perspective of the bathymetry in the study area and location of the Minorca deep station (vertical red line), the ATHAPOC section stations (vertical whites lines) and the ATHAPOC mooring (yellow vertical line). North-South (y), East-West (x), along-slope (y'), and cross-slope (x') axes are included for reference. The x' and y' axes are rotated 38 °(α) counterclockwise relative to x and y.

2005–2017 in order to filter natural noise and to obtain a reasonably smooth, continuous evolution of the hydrographic profiles which can be compared with the theoretical evolution obtained from the 1-D model (see Movie S1 in Piñeiro et al. (2019) to observe a comparison between smoothed and raw profiles).

2.2. The ATHAPOC CTD Section and Mooring

Unfortunately, the initial occupations of the Minorca deep station during the WMT onset period did not include extensive regional, synoptic observations. Instead, cross-slope oceanographic sections carried out in November 2017 and February 2018 (which was also a deep convective period, but much weaker than that in 2005) under the auspices of the ATHAPOC (‘*estudio de la Anomalía TermoHalina en las Aguas Profundas del mediterráneo occidental y su relación con las Oscilaciones Climáticas*’) project provide insight into the impact of deep-water formation on the local hydrographic structure across the continental slope, which cannot be obtained from a single hydrographic station such as the Minorca deep station. Each survey involved a 25-km cross-slope section (40°2.28′ N, 04°25.00′ E – 40°10.92′ N, 04°38.58′ E) of 11 CTD stations that spanned the entire bathymetric range of the continental slope beneath 800 m (white vertical lines in Figure 1b).

Additionally, information on the local circulation patterns of the deep waters over the continental slope of Minorca and changes due to the arrival of newly-formed dense waters in winter 2018 are provided by the ATHAPOC deep mooring, equipped with 3 single-point current meters at 1,000, 1,600 and 2,500 dbar. This deep mooring was installed on the outer continental slope (40°9.64′ N, 04°36.87′ E; yellow vertical line in Figure 1b) and remained in the water between September 2015 and April 2016, and between February 2017 and August 2018, with a sampling period of 30 min.

2.3. Bottom-Intensified Mixing in 2005–2007: Direct Evidence and Working Hypotheses

Visual inspection of the evolution of the deep hydrographic profiles between 2005 and 2007 in the Minorca deep station readily reveals the plausibility of the assumption that motivates this study and generates the working hypotheses.

The remarkable thermohaline structure that emerged in the WMED deep layers as a result of deep convection in the winter of 2005, and its annual evolution during the two following years, is shown in Figure 2.

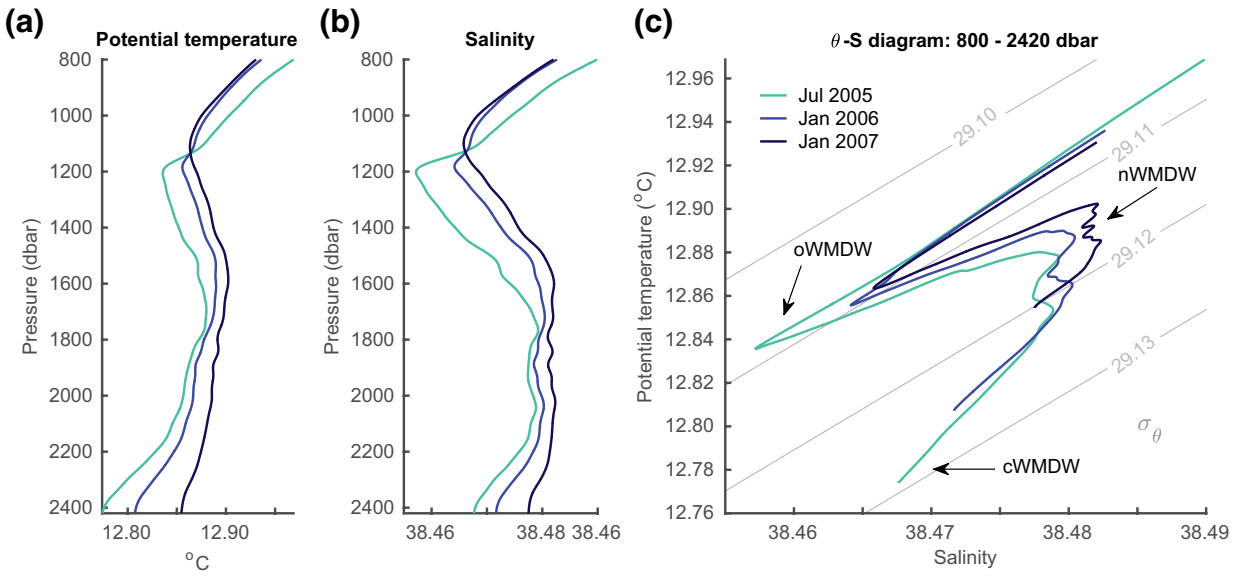

Figure 2. (a) Observed θ profile in July 2005 (turquoise line), January 2006 (blue line), and January 2007 (dark blue line) between 800 and 2,420 dbar at the Minorca deep station. (b) Same as (a) but for S. (c) Same as (a) and (b) but for θ–S. Gray lines denote isopycnal levels (σ_θ).

Beneath the intermediate layers, occupied by the markedly salty and warm Levantine Intermediate Water (LIW; 300–600 dbar), a smoothly stratified thermo-halocline within which θ and S decrease with depth extends toward the fresher and colder oWMDW, which historically occupied the deepest part of the basin. The intrusion of the anomalous WMT dense waters triggered an uplift of the resident deep waters by hundreds of meters and the appearance of a sharp transition around 1,200 dbar, between the oWMDW and the new deep waters (the salty-warm nWMDW and the fresher-colder cWMDW at the bottom). Subsequent profiles in Figure 2 reveal the above-mentioned (i) increase of the θ–S maxima associated with the nWMDW over the 2005–2007 period, and (ii) the significant cWMDW signal erosion.

The rapid fading of the cascading waters in the θ–S plane is still noticeable up to late 2007. Nevertheless, as argued in Piñeiro et al. (2019), observed changes in the water column during 2007 were strongly dominated by large heave of isopycnals (Bindoff & McDougall, 1994) throughout the water column, preventing a description based on our conceptual model based on vertical diffusion and a localized source term. Consequently, the analysis period in this study had to be curtailed to before January 2007. This constraint is addressed in detail in the Discussion (Section 6.1.3).

As stated before, this study focuses on reproducing the thermohaline evolution of the WMED deep waters during the two years following the onset of the WMT as observed in the Minorca deep station, in order to determine whether the erosion of the cWMDW-nWMDW portion signal may be explained by bottom-intensified mixing.

Two hypotheses may be put forward to explain the observed evolution of the cascading waters in the 2005–2007 period:

1. The erosion of the cWMDW-nWMDW segment simply responds to lateral advection of heat and salt within the nWMDW density class, leading to an increase of vertical thermohaline gradients and, consequently, of the downward fluxes of heat and salt toward the deepest layers. In this scenario, no vertical structure in the mixing coefficient needs to be invoked.
2. Lateral advection of heat and salt in the nWMDW class fails to reproduce the observations if a constant mixing coefficient is assumed for the entire water column, such that it is mandatory to model thermohaline evolution with a depth-dependent mixing coefficient in order to match the observations. This would indicate that the rapid erosion of the cascading waters could have been effected by the presence of near-bottom turbulent mixing elevated above background levels.

It is important to note that other combinations can be invoked to explain the observed thermohaline evolution. In particular, drainage of the thermohaline structures cannot be dismissed (i.e., cascading waters leaking from the sampling site toward deeper parts of the basin). Since this study relies on a single hydrographic station, a spatial description is not possible. Nevertheless, this issue will be discussed in depth on the basis of the available knowledge of the post-convective response within the basin.

3. Methodology

To analyze the observed thermohaline evolution of the water column, the one-dimensional diffusion model described by Piñeiro et al. (2019) is used as the starting point. This model provides a theoretical description of the evolution of the θ–S profiles when subject to diapycnal mixing, including double-diffusive mixing schemes. To represent the lateral advection of dense waters formed in the winters of 2005 and 2006, a heat-salt source term is added (the design of this advective term is described in Section 3.1). Finally, the background turbulent mixing coefficient is allowed to vary with depth ($K^{\infty} \equiv K^{\infty}(z)$), so an optimization algorithm is devised to minimize differences between the simulation and the observations while preserving overall consistency (Section 3.3).

3.1. Lateral Advection of Heat and Salt

In order to simulate the increases in θ and S within the nWMDW core induced by the 2005–2006 injections, bulk changes of these tracers in the 2005–2007 period are computed beneath the base of the thermo-halocline

(1,300 dbar). This level is chosen to avoid the oWMDW-nWMDW interface region, which oscillates above ~ 1,200 dbar and is strongly influenced by a downward diffusive heat-salt transfer from intermediate layers. The spatio-temporal structure of the advective source is unknown, so assumptions must necessarily be made.

As regard the vertical (z) distribution of lateral advection, the simplest approach would be to distribute the increases in θ and S homogeneously across a layer of the water column. This option is, however, unrealistic, as newly formed dense waters mix vertically while advected, and also poses computational problems at the boundaries. Since the relative maximum associated with the nWMDW core increases prominently throughout the period, and lacking further information on the shape of the injected anomaly, a Gaussian shape centered at the nWMDW core is a convenient option to represent in a simple fashion the core's erosion as it extends horizontally throughout the basin. With this choice, continuity in the θ–S gradients is then guaranteed. A caveat, which will be addressed below, is that independent injections of heat and salt should not create vertical instabilities, such that further fine-tuning of the source distributions is required.

Assumptions regarding the injection rates of heat and salt into the nWMDW class are also needed. The observational record indicates a smooth increase of θ and S values at the nWMDW core, whereas the physical setting of the process suggests that the two independent convective events in 2005 and 2006 may have provided two distinct advective inputs. Whether the arrival of source waters at the sampling site is actually progressive (i.e., oceanographic processes blur the distinct signatures of the two consecutive deep convection events) or our available observational record is insufficient to disentangle these, cannot be appraised. Therefore, the simplest approach is to add the heat-salt advective column as a decreasing curve throughout the 2005–2007 period, and a more elaborate strategy would be to include the distinct advective pulses (simulating the remnants of the 2005 injection and the following one in 2006). Both of these approaches are analyzed in the simulations in order to explore the robustness of the of the $K^{\infty}(z)$ profile optimization.

3.2. Diapycnal Mixing Parameterization

As the discrete intrusions of the newly formed dense waters in 2005–2006 distorted the original WMT structure observed in July 2005, continuous diapycnal mixing eroded the emergent thermohaline signals and weakened vertical gradients. Turbulent heat-salt fluxes are commonly parameterized following Fick's diffusion equation $\left(\frac{\partial c}{\partial t} = \frac{\partial}{\partial z}\left(K_c(z)\frac{\partial c}{\partial z}\right)\right)$, which can be used to estimate the vertical evolution of the thermohaline tracers (c) over time (t). The rate of mixing is represented by the eddy diffusion coefficient ($K_c(z)$; Klymak & Nash, 2009), usually assumed to be the same for all scalars (θ and S; e.g., Jayne, 2009). Nevertheless, asymmetries between $K_\theta(z)$ and $K_S(z)$ can arise under specific thermohaline configurations of the water column, as a result of the different molecular diffusivities of heat and salt. Portions of the water column prone to developing both forms of these so-called double-diffusive mixing regimes (Kelley et al, 2003; Radko, 2013; Schmitt, 2009), that is, salt fingering and diffusive layering, have been identified throughout the WMT structure (Bryden et al., 2014; Piñeiro et al., 2019).

Thus, to simulate the evolution of the θ and S profiles effected by diapycnal mixing as the lateral advection of dense waters occurs, the one-dimensional diffusion model sensitive to double-diffusive mixing phenomena described in Piñeiro et al. (2019) was adopted. This model vertically integrates the diffusion equation using $K_c(z)$ parameterizations to represent the asymmetries of vertical heat-salt fluxes under double-diffusive and non-double-diffusive mixing regimes. The setting and treatment of advection-diffusion are summarized below. As stated before, the detailed description of the numerical model is provided by Piñeiro et al. (2019).

The spatial domain of the one-dimensional (in z) model is discretized onto a regular vertical grid ranging from depths of 800–2,420 m with a resolution of $\delta z = 10$ m. Using the July 15, 2005 θ–S observed profile as initial condition, at each temporal step ($\delta t = 2.4$ h), the corresponding percentage of the advective column of each tracer (c) is added following the different advective evolution rates, and the mixing regimes throughout the water column are identified by means of a Turner angle analysis (Ruddick, 1983). The one-dimensional diffusion equation is then solved numerically for θ and S using a Crank-Nicolson scheme (Crank & Nicolson, 1947).

The diffusion model is closed by a Neumann boundary condition at the seafloor ($\partial c/\partial z = 0$ at $z = 2{,}420$ m) and by an assimilation scheme at the upper boundary. This time-varying boundary condition is determined by the observed vertical gradients of θ and S in the thermo-halocline, which in turn modulate changes in the vertical heat-salt fluxes toward the deep layers. Data assimilation operates from the upper limit of the vertical domain up to an isopycnal level (29.1088 kg m^{-3}) close to and above the oWMDW-nWMDW interface selected by visual inspection of the hydrographic time series, in order to avoid altering the WMT structure; therefore, θ-S values in the thermo-halocline relax toward observations at these levels. Beneath this region, θ and S evolve as a combination of the lateral advection of heat and salt and the continuous erosion of the thermohaline structure by diapycnal mixing.

$K_c(z)$ within the model is estimated throughout the water column independently for θ and S, using the parameterizations of Zhang and Schmitt (2000) and Zhang et al. (1998), which evaluate the mixing rate as an independent contribution of double diffusion in the regions prone to developing these instabilities ($K_c^{dd}(z)$), and added a constant turbulent background mixing coefficient (K^{∞}) for the entire water column (i.e., $K_c(z) = \left[K_c^{dd}(z) + K^{\infty}\right]$). Contributions from salt fingering and diffusive layering regimes are estimated from the thermohaline gradients according to the parameterizations of Schmitt (1981) and Kelley (1984, 1990). Piñeiro et al. (2019) inferred a depth-independent $K^{\infty} = 4.25 \times 10^{-4}$ m^2 s^{-1} from observations between 2005 and 2017. This coefficient was understood as a regional estimate representative of the average background mechanical mixing levels in the water column off Minorca. The novel additions to the model in this study are the source term at the nWMDW core and the optimization scheme to obtain a best guess of $K^{\infty}(z)$ for the 2005–2007 period.

3.3. K^{∞} Local Optimization

Once the inclusion of the advective term is defined in z and t, we may evaluate whether the observed thermohaline evolution is compatible with a bottom intensification of the mixing coefficient, by optimizing a depth-dependent $K^{\infty}(z)$. We represent a theoretical two-layer structure of $K^{\infty}(z)$, as might be expected from a bottom intensification of the mixing coefficient, through a hyperbolic-tangent idealized target functional shape. This permits representation of the magnitude, location and steepness of the change in mixing coefficient with depth, that is:

$$K^{\infty}(z) = K_b^{\infty} + 0.5\, c_1 \left(\tanh\left(\frac{z - c_3}{c_2} \right) + 1 \right), \tag{1}$$

where $K_b^{\infty} = 4.25 \times 10^{-4}$ m^{2}s^{-1} is the constant background mixing coefficient, c_1 is the maximum increment over K_b^{∞}, c_3 is the center of the hyperbolic tangent, and c_2 refers to the slope at c_3, since it sets the thickness of the transition region between the two layers. The factor of 0.5 forces c_1 to be the maximum increment over K_b^{∞}.

To find the parameters of the $K^{\infty}(z)$ profile that minimize differences between the model and the observations, a combined θ-S normalized root-mean-squared error is defined:

$$\mathrm{RMSE}_{\theta S}^{nor} = (1-\eta) \sum_{i=1}^{n} \frac{(\theta_i^{\mathrm{mod}} - \theta_i^{\mathrm{obs}})^2}{s_\theta^2} + \eta \sum_{i=1}^{n} \frac{(S_i^{\mathrm{mod}} - S_i^{\mathrm{obs}})^2}{s_S^2}, \tag{2}$$

where n is the number of vertical levels considered, θ_i^{mod} and S_i^{mod} are the simulated θ and S values for each depth (z_i), s_θ and s_S are the respective standard deviations of both tracers in the observations (θ_i^{obs} and S_i^{obs}) for a sample of size n (serving as scaling factors accounting for the different variation ranges of both variables in the water column), and η controls the weight of each tracer in the fitting. Here, θ and S are fitted giving equal weight to both, so $\eta = 0.5$ is adopted.

Then, (2) can be minimized numerically by using a Differential Evolution (DE) global optimization algorithm (Chakraborty, 2008; Feoktistov, 2006) that seeks solutions based on linear combinations of the three hyperbolic function (1) parameters. Note that the constant-K^{∞} profile is a particular case in Equation 1 with $c_1 = 0$. Details concerning the algorithm function minimization procedure and the numerical parameters used in this study can be found in the Appendix.

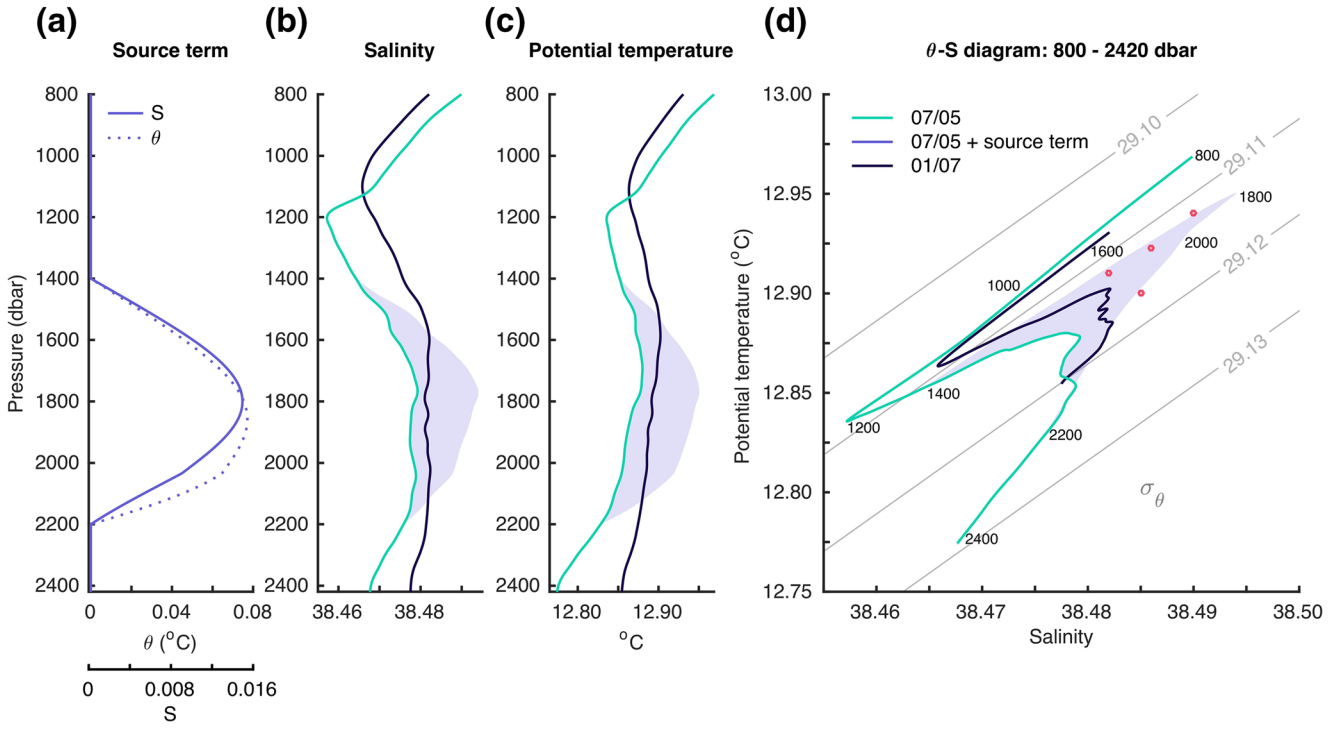

Figure 3. (a) S (purple solid line) and θ (purple dotted line) source terms. (b) Observed S profiles in July 2005 (turquoise line), in July 2005 plus the S source term (combined turquoise-shaded purple area), and in January 2007 (dark blue line). (c) Same as (b) but for θ. (d) Same as (b) and (c) but for θ–S. Gray lines denote isopycnal levels (σ_θ). Red dots refer to reported observations of the nWMDW properties in 2006 in the GoL and Ligurian Sea (Puig et al., 2009, 2013; Smith et al., 2008; Somot et al., 2018). Pressure levels corresponding to the July 2005 profile plus the source term profile are included for reference. Note that the source terms are not completely injected at the start of the simulation, but added progressively.

4. Simulations Setup

Before presenting the results of the complete simulations, it is necessary to precisely define the model setup of the experiments that address the targeted process. Since model outcomes, results, and refined model runs are strongly interrelated, this section shares characteristics between Methodology and Results.

4.1. Source Water Term

Differences in the heat and salt contents below 1,300 dbar between July 2005 and January 2007 indicate that as much as 1.648×10^8 J m^{-2} and 7.494 kg m^{-2} were respectively injected in the deep layers as a result of the 2005–2006 convective events. To include these heat and salt inputs in the simulation, θ–S bulk changes are used to construct the advective water column (Figure 3a). This is done following a Gaussian-shaped distribution, with most of the heat and salt placed in the vicinity of the nWMDW core around 1,800 dbar, whose θ–S maximum increased significantly over the 2005–2007 period. Upper and lower limits of the source term are set at 1,400 dbar and 2,200 dbar, 400 dbar above and below the nWMDW core and spanning the portion of the water column occupied by this deep water mass while preserving the cWMDW-nWMDW mixing line. Within these water column segments, the remaining heat and salt are allocated following the tails of the Gaussian distribution, i.e. diminishing with increasing vertical distance from the core.

Since the evolution of θ and S is considered separately within the model, assuming a theoretical functional shape for the independent advection of both heat and salt requires the resulting advective column to be stable, so that spurious vertical instabilities are not generated that would prevent the diffusive scheme from correctly solving the tracer evolution. Thus, fitting one of the tracers to a Gaussian curve to generate the advective column implies that the distribution of the remaining tracer is constrained by the equation of state. Whereas 100% of the salt is assigned following a Gaussian curve, only 90% of the heat can be normally distributed without generating density inversions. The remaining heat has to be allocated carefully throughout

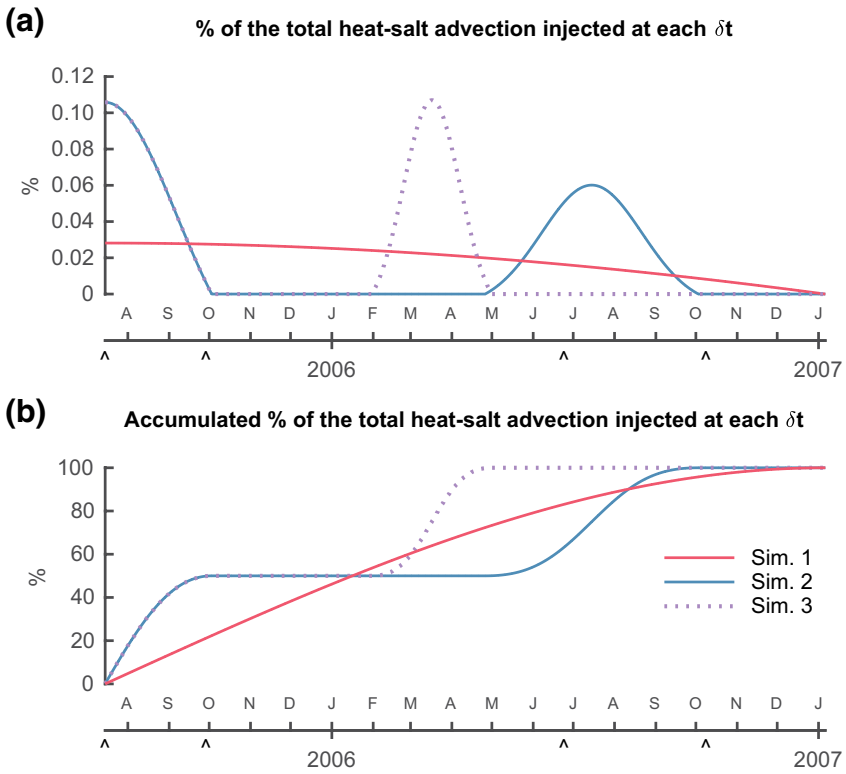

Figure 4. (a) Percentage of the total source term included in the simulation in each temporal step. (b) Accumulated percentage of the source term included in the simulation over time. Vertical arrow tips in the time axes of (a) and (b) indicate the dates in which the Minorca deep station was occupied.

the advective column in order to ensure that stability is preserved. This is performed by successively adding heat (following a Gaussian-shaped distribution) to specific segments of the advective column, selected and recursively smoothed in such a way so that the column remains statically stable. The ensuing distortion of the heat source term can be observed in Figure 3a.

Figure 3 shows the observed θ–S profiles in July 2005 January 2007 and the combination of the former plus the advective term that is introduced in the simulation over time. As expected, the source water core ($\theta = 12.950$ °C, $S = 38.494$, $\sigma_\theta = 29.113$ kg m^{-3}) is located on the isopycnal levels on which the nWMDW evolved, forming a mixing triangle between the three deep water masses with small perturbations around the mixing lines.

The percentage of the advective column that is included in each δt in the simulation varies over time. Figure 4 shows the evolution of the heat-salt input rates under the three assumptions used to represent the arrival of the distinct 2005–2006 injections, which will enable us to test the robustness of the $K^{\infty}(z)$ profile estimation. In all three approaches, a smoothly decreasing curve (Simulation 1) and a double Gaussian shape giving equal weight to each pulse centered on different times (Simulations 2 and 3), lateral advection is restricted to the first year of simulation, adhering to a reasonable spreading time of the newly formed deep waters toward our site. That is, 90% of the heat and salt input is already included in the model by mid-summer 2006, so that the thermohaline evolution of the water column after that time is affected mainly by diffusive mixing processes.

4.2. Vertical Structure of the Mixing Rate

Figure 5 shows the $K^{\infty}(z)$ profiles optimized by the DE algorithm for the 2005–2007 period under the parameterizations used for lateral advection and diffusive mixing in the model. Following the first imposed condition on the advective input rate (i.e., smoothly decreasing over time; Simulation 1) and giving

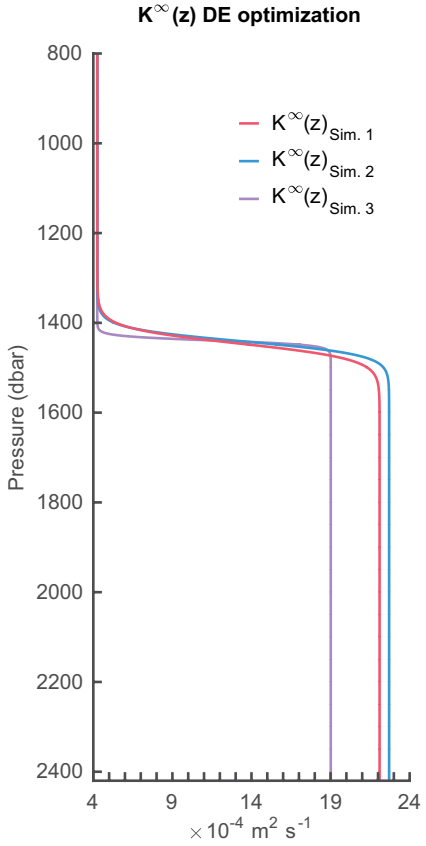

Figure 5. Optimized $K^{\infty}(z)$ profiles for Simulation 1 (red line), Simulation 2 (blue line), and Simulation 3 (purple line).

equal weight to both tracers, minimum errors $RMSE_{\theta} = 0.004$ °C and $RMSE_S = 0.001$ are obtained with $c_1 = 17.84 \times 10^{-4}$ m^2 s^{-1}, $c_2 = 35$ m, and $c_3 = 1{,}446$ m after 300 simulations within the evolutionary algorithm. The resulting $K^{\infty}(z)$ profile shows a prominent increase in the mixing coefficient by about five-fold over the background value, not only within the cWMDW-nWMDW portion but over a thick layer that extends 1,000 dbar above the bottom, coinciding with the upper limit of the source term at 1,400 dbar. The transition between the two layers occurs abruptly in a few tens of meters. Following the advective Gaussian-shaped two-pulse distributions (Simulations 2 and 3) similar minimum errors and hyperbolic function parameters are obtained, replicating the $K^{\infty}(z)$ vertical structure optimized for Simulation 1. Thus, $K^{\infty}(z)$ exhibits little sensitivity to the temporal distribution of the advective pulses. In broad terms, $K^{\infty}(z) \in (19 \times 10^{-4}$ m^2 s^{-1}, 23×10^{-4} m^2 s$^{-1})$ below 1,400 dbar is consistent with reasonable variations in the temporal distribution of lateral advection over the 2005–2007 period. The improvement achieved in the simulations including vertical-varying $K^{\infty}(z)$ instead of the constant-K^{∞} profile is described in the following section.

5. Results

5.1. Simulated 2005–2007 θ–S Profile Evolution

In order to evaluate the realism of the modeled thermohaline evolution under the different assumptions regarding advection and their corresponding optimized $K^{\infty}(z)$ profiles, the outputs of the 540-days simulations are compared with the fortnightly observational set.

For the Simulation 1 (Figure 6 and Movie S1), advection rate is set to smoothly decrease and the corresponding optimized $K^{\infty}(z)$ profile is used (Simulation 1 in Figures 4 and 5). The initial Turner angle profile indicates an intricate succession of mixing regimes in the deep layers (Figure 6d). As the lateral advection of dense water progresses, the vertical configuration of the complex deep-water structure that emerged in winter 2005 is maintained throughout the entire simulation, preserving water column segments prone to developing double-diffusive instabilities. The thermo-halocline region exhibits strong salt-fingering activity ($Tu \approx 87°$), resulting in an asymmetric enhancement of the diffusive coefficients ($K_{\theta} \approx 5.4 \times 10^{-4}$ m^2 s^{-1} and $K_S \approx 6 \times 10^{-4}$ m^2 s^{-1}) and downward heat-salt fluxes (Figure 6e). Beneath the base of the thermo-halocline, diffusive layering operates ($Tu \approx -81°$), transporting heat upward more efficiently than salt ($K_{\theta} \approx 4.4 \times 10^{-4}$ m^2 s^{-1} and $K_S \approx 4.3 \times 10^{-4}$ m^2 s^{-1}). Even though the entire oWMDW-nWMDW portion (1,200–1,700 dbar) is prone to moderate-to-strong diffusive layering activity, its effect is barely noticeable due to the background turbulent mixing intensification beneath 1,400 dbar. The impact on vertical heat-salt fluxes of moderate salt fingering ($Tu \approx 69°$) operating in the cWMDW-nWMDW portion is likewise negligible for the overall thermohaline evolution in the deepest part of the water column, which is also dominated by background turbulent mixing.

Discrepancies between the observational record and model runs are expected. The observed evolution of the nWMDW core progressively gained heat and salt within the modeled period while preserving a double θ–S maximum, which the model rapidly eroded. Such double maximum was caused by transient structures captured by the raw observational record and that cannot be accounted for in an exercise aiming to understand the general hydrographic evolution of the water column from simple theoretical premises.

Overall, the θ–S profiles evolve similarly to the measured hydrography, and after 540 days model outputs match the observations reasonably with maximum θ (°C) and S differences of $\mathcal{O}(10^{-3})$ below 1,210 dbar (the maximum pressure reached by the assimilation term. Figures 6a, 6b, and 6f). The evolution of the density structure is also reproduced satisfactorily (Figure 6c). Erosion of the cascading waters is slightly

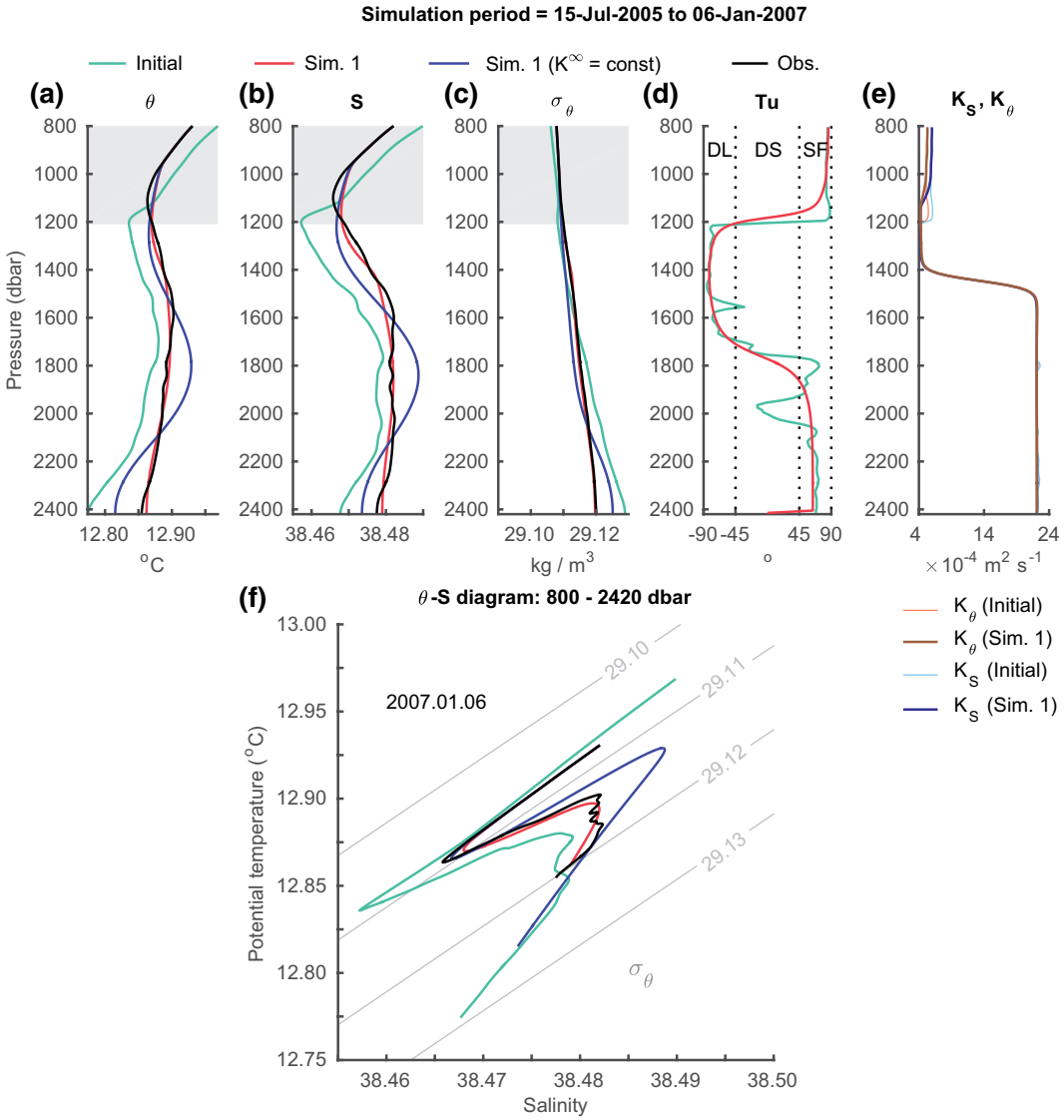

Figure 6. (a) θ profile evolution between July 2005 and January 2007 (800–2,420 dbar). The initial profile is shown by the turquoise line. Observed (black line), Simulation 1 (red line), and Simulation 1 with constant $K^{\infty}(z)$ (blue line) profiles in January 2007 are also shown. Shaded areas indicate the maximum assimilation pressure range during the simulations. (b) Same as (a) but for S. (c) Same as (a) and (b) but for potential density anomaly (σ_{θ}). (d) Turner angle in Simulation 1 in January 2007 (red line) and for the July 2005 initial profile (turquoise line). Dotted vertical lines delimit the three mixing regimes: salt fingers (SF), diffusive layering (DL) and doubly stable (DS). (e) K_{θ} (brown line) and K_S (dark blue line) profiles in Simulation 1 in January 2007, and initial K_{θ} (thin orange line) and K_S (thin light blue line) profiles. (f) Same as (a), (b), and (c) but for θ-S. Gray lines denote isopycnal levels (σ_{θ}). For the complete simulation, the reader is referred to Movie S1.

more prominent in the simulation than observed, resulting in a warmer and saltier 29.12 kg m^{-3} isopycnal occupying the bottom of the water column in January 2007.

For reference, the modeled evolution of the thermohaline profiles using a constant $K^{\infty}(z) = 4.25 \times 10^{-4}$ m^2 s^{-1} is also shown in Figure 6. Lateral advection of heat and salt during the 2005–2007 period causes a pronounced increase of the nWMDW θ–S relative maxima and a subsequent enhancement of the vertical gradients in the transition regions between water masses. In the absence of vertical structure in the mixing coefficient, the increased heat-salt vertical fluxes are not intense enough to effectively erode the θ–S maxima, ultimately producing a markedly warmer and saltier nWMDW and a weaker erosion of the cWMDW-nWMDW signal at the end of the simulation.

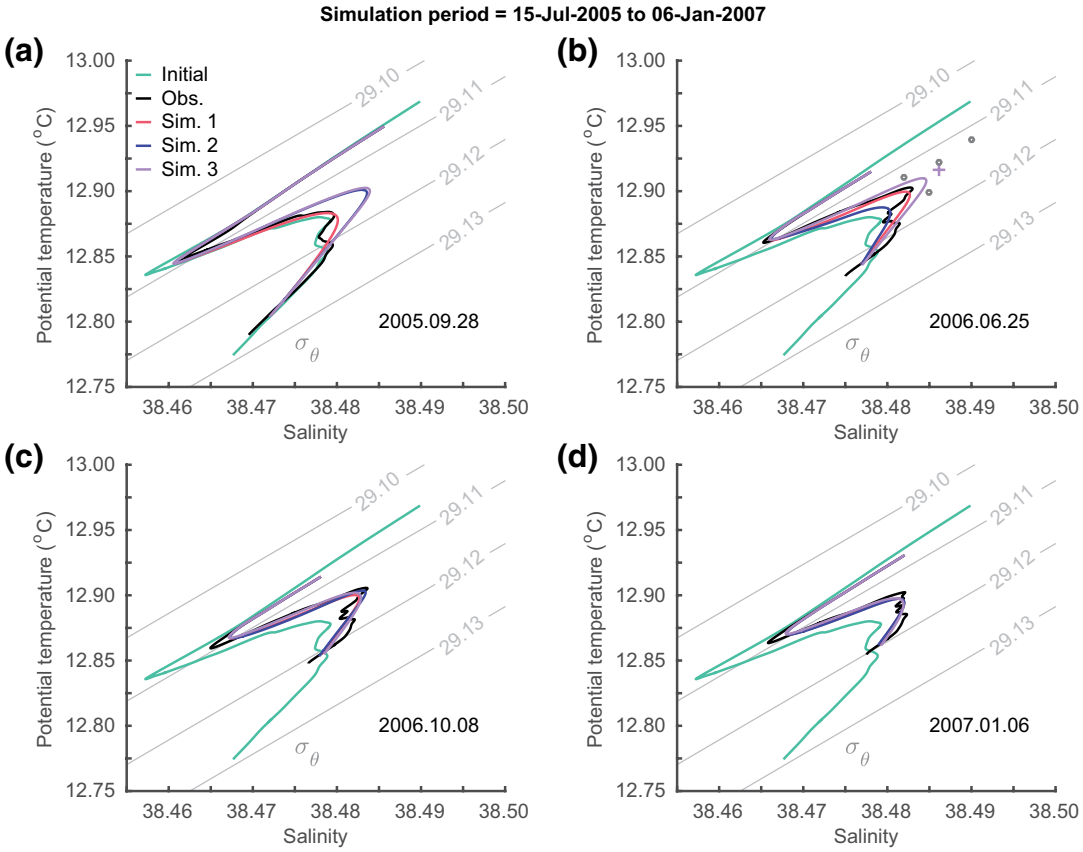

Figure 7. (a) θ–S profile evolution between July 2005 and September 2005 (800–2,420 dbar). The initial profile is shown by the turquoise line. Observed (black line), Simulation 1 (red line), Simulation 2 (blue line) and Simulation 3 (purple line) profiles in September 2005. (b) Same as (a) but in June 2006. Gray dots refer to reported observations of the nWMDW properties in 2006 in the GoL and Ligurian Sea (Puig et al., 2009, 2013; Smith et al., 2008; Somot et al., 2018). Purple cross indicates nWMDW core properties in April 2006 in Simulation 3. (c) Same as (a) and (b) but in October 2006. (d) Same as (a), (b) and (c) but in January 2007. Gray lines in (a), (b), (c), and (d) denote isopycnal levels (σ_θ).

Observations between 2005 and 2007 are therefore compatible with a lateral advection of heat and salt in the nWMDW density levels and a deep intensification of the background mixing coefficient. Using different approaches to represent the evolution of the advection rate, similar optimized $K^{\infty}(z)$ profiles and errors are obtained. Imposing a decreasing advection rate is the most straightforward approach given the impossibility of extracting further information from the temporally sparse observations, but the distribution of the lateral source term into two discrete pulses is conceptually more adequate to realistically represent the arrival of dense water formed in the convection area during winter. The comparisons between simulations, the observations on the dates when the Minorca station was actually occupied (i.e., those underpinning the interpolated dataset; see vertical arrow tips in Figure 4) and the observed final θ–S profile on 6 January 2007 are synthesized in Figure 7. On the whole, the observed evolution is correctly reproduced using a smooth progression of the input rate (Simulation 1). Giving the same weight to the pulses in 2005 and 2006 (Simulations 2 and 3), θ-S profiles are noticeably mismatched from the observations in September 2005, as they overestimate the remnants of the 2005 injection. By June 2006, Simulation 3 (second pulse centered in March 2006) reproduced more accurately the observations than Simulation 2 (second pulse centered in July 2006), suggesting a rapid arrival of the newly-formed deep water to Minorca. During the closing months of the time series, all simulations evolve according to the observations. In all cases, the optimized $K^{\infty}(z)$ is similar between the three simulations, thus indicating low sensitivity to the temporal evolution of the lateral advection.

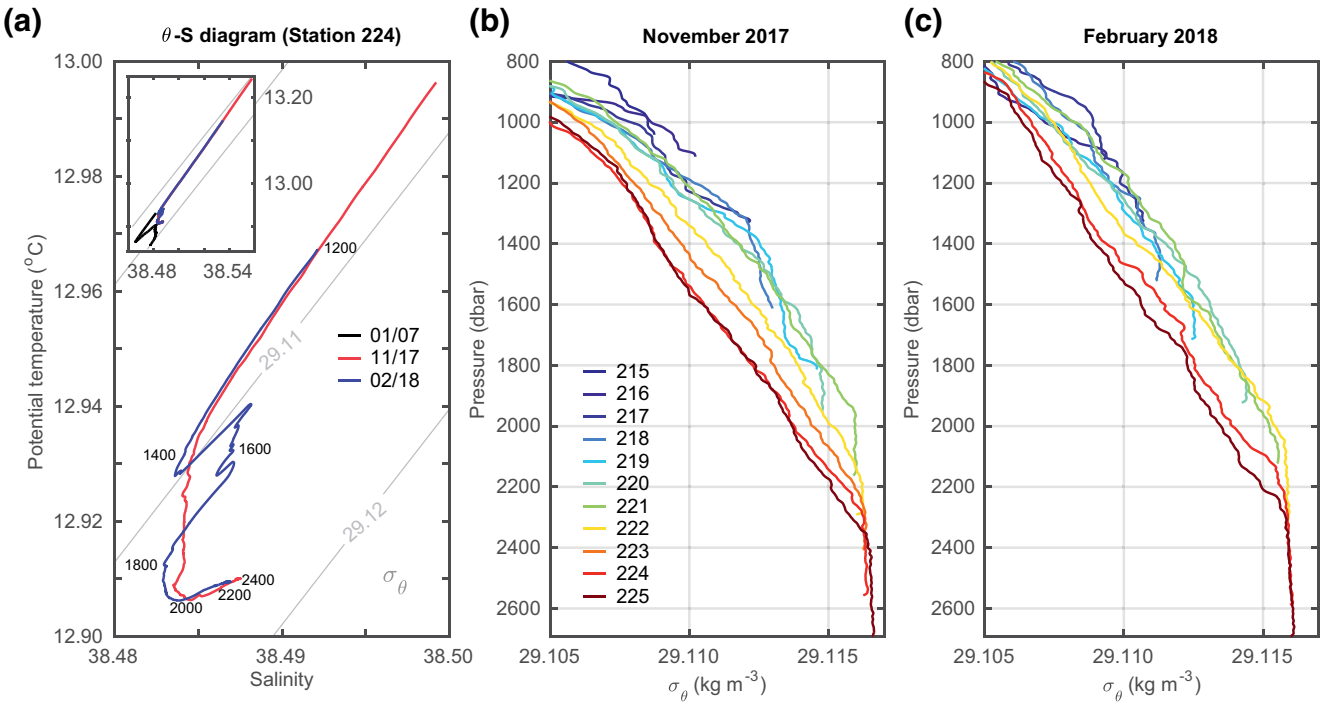

Figure 8. (a) θ–S diagram at station 224 (beneath 1,200 dbar) in November 2017 (red line) and in February 2018 (blue line). Gray lines denote isopycnal levels (σ_θ). Pressure levels corresponding to the February 2018 profile are included for reference. Inset diagram in (a) shows a comparison between θ-S profiles beneath 800 dbar in November 2017 (red line) and February 2018 (blue line) at station 224, and January 2007 (black line) at the Minorca deep station. 29.10 kg m^{-3} and 29.12 kg m^{-3} isopycnal levels are included. (b) Potential density anomaly (σ_θ) profiles (800–2,694 dbar) of the ATHAPOC section in November 2017. (c) Same as (b) but in February 2018. The profile color denote the station number (see locations in Figure 1b).

5.2. Slope Density Structure and Circulation During Winter 2017–2018

Intensive hydrographic and current meter observations in the study area (Figure 1b) over the deep convective winter of 2017–2018 offer further insights into regional dynamics associated with the lateral advection of newly-formed dense waters toward the Minorca site.

The θ–S diagram (Figure 8a) beneath 1,200 dbar in November 2017 shows the presence of much warmer, saltier and lighter deep waters than those occupying the deepest parts of the basin in 2005–2007. The original thermohaline signature of the WMT is no longer present, and only a warm and salty tongue perturbs the bottom of the θ–S profile (see Piñeiro et al. (2019) for the complete description of the thermohaline evolution within the period). Beneath 800 dbar, profiles along the cross-slope section show a generalized off-shore density reduction over isobaric levels, indicating an on-slope piling of the deep waters (Figure 8b). Maximum densities of 29.116 kg m^{-3} were recorded in the outermost stations of the section, in quasi-homogeneous bottom layers that extended 300 dbar above the bottom. Additional homogeneous layers of differentiated density in on-slope profiles indicates the presence of bottom boundary layers (BBLs) more than a hundred meters thick that are distinct from the weakly-stratified ambient bottom water mass (Figure 8b).

In February 2018, a new deep structure emerged in the θ–S diagram between 1,400 and 1,800 dbar as a result of the lateral advection of newly-formed dense waters, creating new relative maxima of θ and S in the deep layers (Figure 8a). Density profiles along the hydrographic section show significant changes compared to November 2017. The outermost stations recorded density inversions of tens of meters throughout the water column portion where the dense water intrusion occurred, especially notable at station 224. Furthermore, new BBLs in on-slope profiles coinciding with that pressure range were registered, as well as a generalized reduction of density in the BBLs that were observed in 2017 (Figure 8c).

Circulation patterns in the outer continental slope of Minorca were captured by current meter measurements between September 2015 and August 2018 in the ATHAPOC mooring site, which show that the deep boundary circulation is characterized by a predominantly southward flow (Figure 9a). About 75% of all ob-

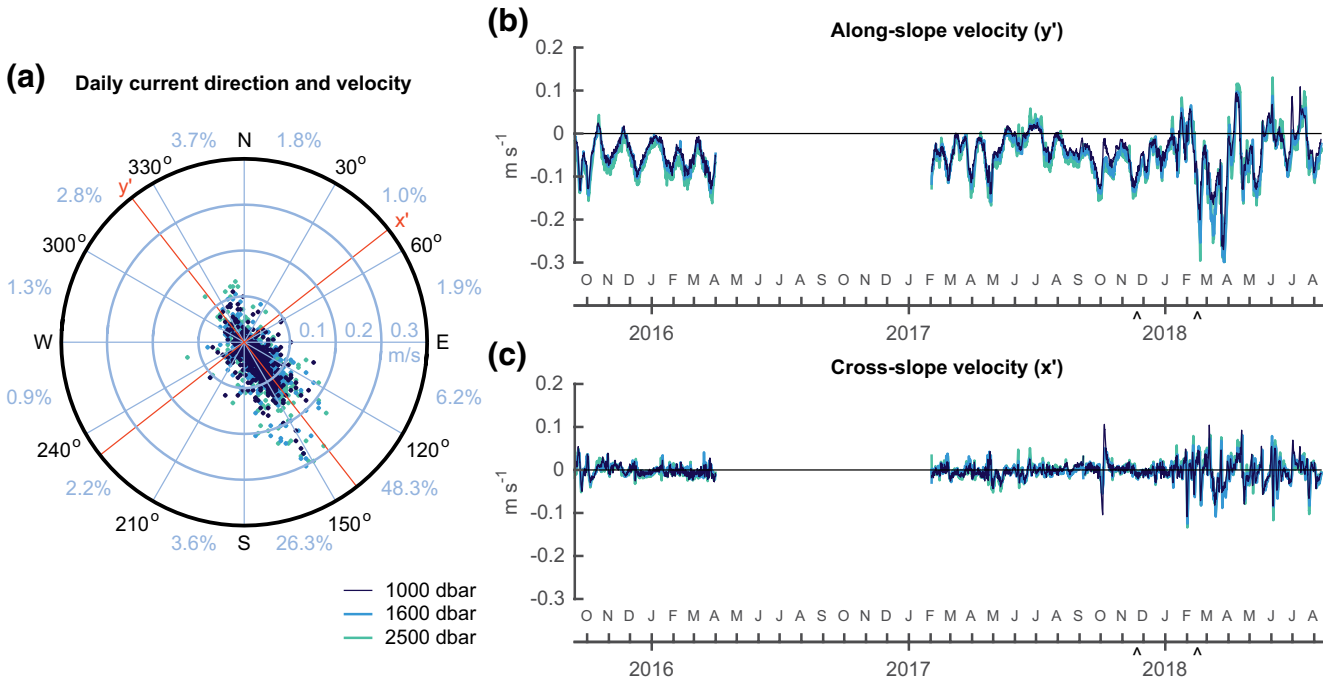

Figure 9. (a) 24-h low-passed daily current direction and velocity at 1,000 dbar (dark blue dots), 1,600 dbar (light blue dots) and 2,500 dbar (turquoise dots) at the ATHAPOC mooring site (see location in Figure 1b). Red axes refer to cross-slope (x') and along-slope (y') directions. Percentages of the total observations for each direction range are included for reference. (b) Along-slope component at 1,000 dbar (dark blue line), 1,600 dbar (light blue line) and 2,500 dbar (turquoise line). (c) Same as (b) but for cross-slope component. Vertical arrow tips in the time axes of (b) and (c) indicate the dates on which the ATHAPOC section was occupied.

servations were directed toward the S-SE ($\overline{v}$ = 0.07 m/s), following the longitudinal axis of the continental slope. Records at 1,000, 1,600, and 2,500 dbar reveal a depth-intensification of the current, with maximum velocities of 0.3 m/s. Decomposing current time series into cross-slope and along-slope components (38° anticlockwise rotation; see Figure 1b) yields (Figures 9b and 9c). As expected, along-slope circulation dominates over the cross-slope component, with a stable southward flow of varying intensity that appears to periodically oscillate throughout the 2015–2018 period. Cross-slope velocities exhibited more variability, with recurrent swings between on-slope and off-slope directions. Maximum intensification of the along-slope current occurred during three depth-intensified strong pulses of 2–3 weeks each between February and March 2018, coinciding with the deep-water formation period and the intrusion of dense water detected in station 224 (Figure 8). From then until the end of the time series in August 2018, the intensity and variability of both current velocity components increased markedly.

6. Discussion

The evolution of the complex hydrographic structure emerging after the WMT onset in the deep waters off Minorca Island is consistent with a rather simple conceptual study, explored through a numerical model in which a source term modulates nWMDW heat-salt advective gains and the background mixing coefficient is enhanced near the bottom. In this section, we will discuss the robustness of the assumptions behind the one-dimensional simulation that supports this study, the discrepancies between the observed and simulated evolution and their possible causes, and the insights that can be drawn on deep-ocean mixing dynamics over the continental slope of Minorca during the post-convective periods.

6.1. Simulation of the 2005–2007 θ–S Evolution in the Deep Waters

6.1.1. Source Term Properties

Propagation of newly formed dense waters from the convection area toward Minorca implies the advection of vertically heterogeneous water columns that evolve by mixing with the surrounding waters as they spread throughout the basin. Since the simulation of the thermohaline evolution of the deep layers over 2005–2007 depends on an ad hoc heat-salt source conveniently injected into the July 2005 initial profile, a first question that should be addressed is whether the idealized source term reasonably represents known properties of the dense-water formation in 2005–2006.

The heat and salt lateral advection source term was concentrated around the nWMDW core, that is, beneath the thermo-halocline and above the cWMDW-nWMDW class. The rationale of this choice is that the observed evolution of the θ–S diagram indicates a strong pull from warmer and saltier water at around the 29.115 kg m^{-3} isopycnal, in accordance with the observed 2006 nWMDW characteristics in the Ligurian Sea and the GoL area (Figure 3d; Puig et al., 2013, 2009; Smith et al., 2008; Somot et al., 2018). Likewise, it is known that dense shelf waters barely modified the background characteristics of the deep water in winter 2006 (Fuda et al., 2009; Puig et al., 2013; Schroeder et al., 2013). Dedicated simulations revealed that the newly-formed dense waters in winter 2005 reached densities of 29.10–29.13 kg m^{-3} and a formation density threshold of 29.12 kg m^{-3} the following winter (Beuvier et al., 2012; Somot et al., 2018), not inconsistent with our choice of density classes in which the source term adds heat and salt in the simulation, that is, 29.110–29.124 kg m^{-3} (Figure 3).

6.1.2. Biases Associated with Cascading Water Sources

As outlined above, the intensity of the cascading water signal is maximum at the start of the record (lowest θ and S at the bottom of the water column) and the 2006 cascading event was not reported to generate a conspicuous dense water mass as in 2005, so we assume no further specific cascading water sources at these levels in our simple model. Nevertheless, a careful look at the evolution of the cWMDW-nWMDW water column segment shows a subtle deviation from the straight mixing line that would be expected from diffusion (Figure 2). The actual evolution of heat and salt in the deepest part of the water column simulated by the model is slightly warmer and saltier on the near-bottom isopycnal levels in 2007 than observed (Figure 7); thus, a modest contribution of cascading waters in 2006 may be an explanation for this mismatch.

It is important to emphasize that, although the observations are *consistent with* the model constraints that we have defined (advection at nWMDW and enhanced deep mixing), this is not the only possible explanation of the observations. In particular, we are not considering the possible drainage (via advection) of deep cascading waters within the simulation period. If such a drainage was considered, the mixing coefficient required to match the observations would depend on the magnitude of the cascading water source/sink. This possibility cannot be explored without a three-dimensional model and precise knowledge of horizontal property distributions. However, a simulation of the spatio-temporal evolution of the deep waters formed in the winter of 2005 by Beuvier et al. (2012) suggests that dense cascading waters were effectively eroded while circulating off Minorca in less than a year. While those authors argue that the waters' spreading velocities may be underestimated in their model, observations of the anomalous WMT structure in the central abyssal plain between Minorca and Sardinia in April–May 2005 (Schroeder et al., 2006) and in the Algerian sub-basin in the subsequent early-summer (López-Jurado et al., 2005; Schroeder et al., 2008) do not exhibit bottom waters denser than 29.125 kg m^{-3}, thus endorsing the notion of a strong local consumption of the dense cascading waters off the continental slope of Minorca. In any case, the erosion of cWMDW at our observation site may be explained exclusively by mixing with overlying waters.

6.1.3. The Post-Convective Third Year: The Heave Issue

By construction, the model constrains the hydrographic evolution to arise from a combination of diapycnal mixing and a localized source term that simulates the advective arrival of distinct water masses. Therefore, our scheme does not account for hydrographic changes due to the vertical displacement of isopycnals, known as heave (Bindoff & McDougall, 1994). Heave-induced changes preserve the θ–S diagram while altering the volumetric expression of different water masses, and are commonly caused by dynamical factors (e.g., perturbed currents driving a shift of isopycnal levels, or the lateral translation of a large-scale gyre).

Heave is thus an issue that must be considered in our attempts to isolate the hydrographic signatures of diffusive processes in a single hydrographic station. Piñeiro et al. (2019) used the constant K^{∞}-only version of the present model to analyze the long-term evolution of the deep waters over 2005–2017, seeking to disentangle advective versus diffusive contributions. Advective effects due to the formation of new water types clearly emerged in years when deep convection occurred, but other years (like 2007) when no deep-water formation was identified also exhibited heat-salt content changes of advective origin in the deep layers, mostly linked to the vertical displacement of the overall water column structure (i.e., heave).

In 2007, strong heave pushed downwards the oWMDW-nWMDW interface, as well as the underlying water masses. The overall deepening of isopycnals that year was interpreted as a large-scale dynamical effect, related to post-convective rearrangement of water masses following major deep-water formation events. The isopycnal deepening was associated with a reduction in near-bottom density, suggesting to stem from a leakage of the densest resident waters toward the deepest parts of the basin (Piñeiro et al., 2019). At any rate, from early 2007 onward, the strong heave present in the record invalidates our modeling premises. Indeed, attempts to simulate this period with the adopted model setup and $K^{\infty}(z)$ optimization were fruitless. $K^{\infty}(z)$ estimated under strong heave is not only meaningless, but it is also not possible to satisfactorily reproduce the observed hydrographic evolution.

6.1.4. Bulk Heat and Salt Content: Advection Versus Diffusion

The net lateral advection of heat and salt into the deep layers was estimated from the bulk differences between the observed profiles in July 2005 and January 2007 beneath 1,300 dbar. This direct calculation is likely to underestimate the advective terms, since it doest not take into account the upward diffusion of heat and salt out of this domain. Simulated profiles in January 2007 display a heat and salt content deficit of 4×10^6 J m^{-2} and 0.6711 kg m^{-2} when compared to the observations (Figure 7). Therefore, the advective term should have been 2.4% and 8.9% warmer and saltier to balance such a heat and salt leakage.

Piñeiro et al. (2019) estimated the advective contributions to the evolution of the deep layers' heat and salt content between 2005 and 2017 off Minorca, by calculating the differences between the observed profiles (i.e., those underpinning the interpolated dataset) and the evolution that each profile would have followed up to the next profile if only diffusion was operating. Accounting for the diffusive leakage of heat and salt toward the oWMDW-nWMDW interface, computed in this way, yields a mismatch error reduced to about 0.6%.

A more rigorous approach would thus be to re-run the model with slightly enhanced advective sources and apply further corrections recursively, since the transfer of heat and salt depends on the simulated evolution of the hydrographic profiles. This further tuning has no significant impact on either the simulated evolution of the thermohaline structure or the estimated $K^{\infty}(z)$. Accordingly, no further corrections were implemented, in order to avoid adding unnecessary complexity.

6.1.5. Advective Inputs of Newly Formed Convective Waters

The evolution of source water inputs to the sampling site is not well captured by the relatively sparse hydrographic record, so up to three plausible distinct temporal distributions of the source water injection were defined in order to test the robustness of the K^{∞} profile optimization (Figure 4). The model's final outcome is rather insensitive to source water function choice, that is, all the distributions provide similar vertical profiles of the mixing coefficient. However, the modeled intermediate stage deserves further analysis (Figure 7). Simulations using two equally weighted advective pulses in 2005 and 2006 overemphasize the remnants of the 2005 injection, which are nearly fully integrated into the initial profile of July 2005. The θ–S profile in July 2006 is well reproduced when the 2006 injection is centered in March (Simulation 3) and not in April-October (Simulation 2), once the deep-water formation period in the GoL is concluded (Somot et al., 2018). Further, nWMDW-core θ and S in late winter of 2006 in Simulation 3 are in close agreement with reported observations of the nWMDW characteristics in the convection area (see purple cross and gray dots in Figure 7b), suggesting that the source term is representative and that newly-formed deep waters spread rapidly toward our site.

Schroeder et al. (2008) documented the spreading of the 2005–2006 anomaly from repeated CTD stations throughout the basin. By April-May 2005, the deep structure of the WMT was apparent in the θ–S diagrams

to the east and south of the Balearic Islands and traceable in the Algerian basin, reaching the entrance of the Alboran Sea in less than 6 months. By late 2006, the anomaly was detectable all over the basin. Estimates from CTD and current meter data in 2018 off Minorca show the same rapid spread of newly formed deep waters. Persistent near-bottom peak velocities of 0.15–0.40 m/s are commonly reported on the Catalan continental slope and in the GoL abyssal plain (e.g., Durrieu de Madron et al., 2017, 2013; Houpert et al., 2016; Salat et al., 2010) during the post-convective stages, as deep waters leave the convection area with the along-slope boundary current and are transported into the basin interior by submesoscale eddies (Send et al., 1996; Send & Testor, 2017; Testor & Gascard, 2003, 2006). These velocities are similar to those recorded off Minorca in winter 2018 in association with dense waters flowing south-eastward into the Algerian sub-basin. Assuming a sustained propagation at 0.15–0.30 m/s between the formation area and our site, newly formed dense waters would arrive at the continental slope off Minorca in less than one month. Therefore, signatures of distinct newly-formed dense waters quickly arriving at our sampling site within each deep convective year should be noticeable in the hydrographic profiles. A higher sampling rate is required to confirm this in future deep-water formation events.

6.2. Bottom-Enhanced Mixing during the Post-Convective Stages

From consecutive observations with a marked diffusive behavior, Piñeiro et al. (2019) estimated a depth-independent coefficient for the entire water column of $K^{\infty} = 4.25 \times 10^{-4}$ m^2 s^{-1}, which was considered representative of the mean level of mechanical mixing in the region. In this study, we find the evolution of the hydrographic structure during the convective and post-convective stages of the 2005–2007 period to be best described by a $K^{\infty}(z)$ profile with a sharp increase from ~ 1,400 dbar to the bottom, where the mixing rate is five times larger than the previously estimated local background diffusivity (Figure 5).

Since the present study was motivated by the rapid erosion of the cascading water properties, it is somewhat surprising that the observed thermohaline evolution cannot be satisfactorily reproduced with a mixing intensification restricted to near the bottom, where the cascading waters lie. Instead, the layer of elevated turbulence extends 1,000 dbar above the bottom, coinciding with the upper limit of the source term beneath the base of the thermo-halocline. Thus, enhanced diapycnal fluxes of heat and salt in the deep layers effect a more efficient transfer of the laterally advected properties throughout the water column, leading to a rapid erosion of the intruding signals (see red and blue lines in Figure 6).

While the representativeness of the imposed temporal distributions of lateral advective sources and the suitability of a temporally invariable $K^{\infty}(z)$ profile may be debated, our results robustly indicate that the dense waters injected in 2005–2006 experienced persistent, intense diapycnal mixing. Evidence of such strong mixing has not been reported so far in observations or estimates from previous ocean mixing studies in the WMED basin interior. Our estimated $K^{\infty} \sim 22 \times 10^{-4}$ m^2 s^{-1} in the deep layer greatly exceeds the upper limit of reported values in the deep WMED interior, which are in the range 0.1–10 $\times 10^{-4}$ m^2 s^{-1} (Cuypers et al., 2012; Ferron et al., 2017), as well as characteristic mixing rates beneath the permanent thermocline of the global ocean (Waterhouse et al., 2014). Thus, the occurrence of this intense deep mixing calls for further discussion.

Local intensification of turbulent mixing is commonly observed in association with shear stresses at the seabed, and results in well-mixed bottom boundary layers (BBLs) that can extend tens of meters above the bottom (Lueck, 2001). The deep amplification of $K^{\infty}(z)$ in our model spans well above the vertical range where intense mixing might be expected to be sustained by locally generated near-bottom turbulence. Indeed, the presence of BBLs in the four actual observations that underpin our interpolated record is intermittent and detectable at most up to 60 m above the bottom. This suggests that the intense mixing required to explain the observed hydrographic evolution off Minorca during 2005–2007 does not reflect an in situ mixing process, but may be the signature of well-mixed waters being laterally advected toward our site.

The continental slope of Minorca is regarded as a plausible source of the mixing necessary to reproduce the 2005–2007 observations. Topographic stress generated by a steady flow along a sloping boundary produces an associated downwelling Ekman transport if the background flow is in the direction of Kelvin wave propagation (Benthuysen & Thomas, 2012). The bottom Ekman transport across isobaths advects relatively light water beneath denser waters, rendering stratification unstable and triggering convective instabilities. The

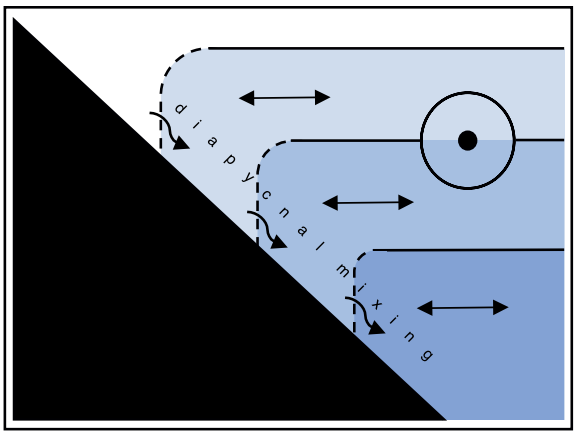

Figure 10. Schematic of the deep boundary mixing mechanism developing over a linear topographic slope. Solid contours indicate density surfaces and dashed lines indicate the weakly stratified bottom boundary layer (BBL). The direction of the background flow is denoted by the circled dot. Topographic stress induced by the boundary current triggers a downwelling Ekman transport of relatively light waters across the BBL, enhancing diapycnal mixing. Lateral exchange between well-mixed near-boundary layers and the stratified interior advects away the effects of the topographically localized water transformations.

ensuing mixing over the sloping bottom induces a tilt of isopycnals and a thickening of the BBLs, which have been suggested to act as hotspots for water mass transformation in the abyssal ocean (Ferrari et al., 2016). Recently, boundary-interior communication of the effects of such topographically localized turbulence associated with a Southern Ocean deep current flowing along a sloping bottom was thoroughly documented by Naveira-Garabato et al. (2019) (Figure 10), who reported large K^{∞} values in the near-boundary region comparable to those estimated with our optimization-based approach. The occurrence of such a deep boundary mixing in the continental slope of Minorca is explored by means of the ATHAPOC CTD cross-slope high-resolution section and mooring, which captured the arrival of newly-formed dense waters in winter 2018, over a decade after the WMT onset.

Hydrographic and current data gathered above the continental slope of Minorca during 2017–2018 exhibit a range of features indicative of the deep-ocean mixing mechanism documented in the Southern Ocean. Current meter data during 2015–2018 show that the general circulation pattern over the continental slope is characterized by a depth-intensified, predominantly southeastward flow that follows the longitudinal axis of the continental slope (Figure 9a), in line with the deep cyclonic circulation of the WMED basin (Send & Testor, 2017). In February-March 2018, the along-slope velocity intensified to values of 0.3 m/s in three distinct episodes (Figure 9b), and lateral advection of newly-formed dense waters is evident at the outer continental slope (Figure 8). The expected response in the density structure due to the topographic stress associated with the intensified along-slope flow may be registered in the on-shore stations in February 2018, which show the occurrence of new thick BBLs (not present in the November 2017 profiles) coinciding with the isobaric range where the intrusion's core was detected in the off-shore station (Figure 8). Interestingly, cross-slope velocity variability and intensity increased markedly following the along-slope transport of the newly formed dense waters until the end of the time series in August 2018 (Figure 9c). This is compatible with the lateral exchange of well-mixed boundary layers that effectively propagates the effect of the BBL turbulence away from the sloping boundary (Naveira-Garabato et al., 2019). The overall sequence observed in winter of 2018 is, thus, plausibly consistent with intensified bottom boundary mixing over the continental slope induced by the enhanced along-slope circulation that follows deep-water formation in the GoL area. This deep-ocean mixing mechanism is expected to have been operating after the much more dramatic deep-water formation events in 2005 and 2006, and could explain the strong deep mixing diagnosed by our optimization procedure in the outer continental slope off Minorca during the WMT initial stages. A future targeted study of boundary mixing in this region is called for to corroborate and develop the indicative evidence presented here.

7. Conclusions

Hydrographic time series from a regularly occupied deep station in the outer continental slope off Minorca enables to trace the changes in the WMED deep layers following the appearance of the WMT thermohaline structure in the winter 2005, up to the present day. The rapid erosion of the original WMT near-bottom hydrographic structure, observed during the first 2 years of the record, is shown to provide evidence of regional bottom-intensified mixing. The local evolution of the WMT hydrographic structure during 2005–2007 was reproduced through a combination of lateral advection of dense waters and diapycnal mixing, using a one-dimensional diffusion model with a source water term that encapsulates our current knowledge of dense-water renewal in the area. An optimization algorithm was adopted to infer a depth-dependent turbulent mixing rate.

We find that almost the entire water column influenced by the WMT experienced persistent, intense mixing greatly exceeding previous rates estimated for the region, and not only in the densest waters. As no indica-

tion of such a vertically extensive, local depth-intensified mixing can be obtained from the observations, ex situ mixing of the deep waters and subsequent transport toward our site was considered. New hydrographic and current measurements above the continental slope off Minorca in the winter of 2018 show evidence of mixing intensification near sloping topography as along-slope flow of newly formed dense waters occurs. This suggests that strong boundary mixing and lateral export is a plausible source of the remarkably intense and extensive deep-water transformation inferred during the 2005–2007 period offshore Minorca Island.

This study advances our knowledge of the WMT evolution during its initial stages, and points to a boundary mixing mechanism not previously described in the WMED. A dedicated investigation of this mechanism will be the subject of future work.

Appendix A: DE global optimization algorithm

The best guess of the $K^{\infty}(z)$ profile is obtained by means of a DE global optimization algorithm which finds the parameters of 1 that minimize errors between the observed θ and S profiles and the simulation. DE is an iterative method, not derivate-based, which use a population of individuals, here representing the parameters of 1, that evolves generation by generation toward the solution that minimizes the objective function. The algorithm operates as follows:

Initially, a random population of size m, is generated in the search space. Every individual, $j \in [1, m]$, is defined by a vector $v_j = [c_{j1}, c_{j2}, c_{j3}]$ which contains a value for each parameter of 1. For every j, a fit value is also defined, g_j, in our case the error computed by means of 2. At every generation, the best individual (b) in the population that satisfies $g_b = \min(g_j)$ for all j is identified. The initial values for v are taken from a uniform distribution between two limits for each parameter:

$$v_j = L_j^{\min} + (L_j^{\max} - L_j^{\min})U[0,1). \tag{A1}$$

In our case, appropriate values for theses limits were: $c_1 \in [0.0010, 0.0040]\ \mathrm{m^2\,s^{-1}}$, $c_2 \in [10, 100]$ m and $c_3 \in [z_{\min}, z_{\max}]$, where $z_{\min}$ and $z_{\max}$ correspond to the upper and lower limit of the vertical domain of the simulation.

There are several variants of DE. In this study, DE/current-to-best/1 scheme was used. The evolution process at each generation, $ig \in [1, ng]$, follows the algorithm:

1. ig is increased in 1. The fit, g_j, of every individual, j, is then calculated, and the best one, b, is detected.
2. For each individual, j, two individuals are randomly selected $k_1, k_2, j \neq k_1 \neq k_2$, and the following calculation is performed:

$$u_{jl} = (1 - \mu)v_{jl} + \mu v_{bl} + F(v_{k_1 l} - v_{k_2 l}), \tag{A2}$$

   where F is a mutation factor and μ is the weight of the best individual in the mixing (A2). $l \in [1, 3]$ refers to each parameter of function (1) defining v_j.
3. A crossover is carried out, depending on a probability, CR, by

$$w_{jl} = \begin{cases} u_{jl}, & \text{if} \quad x_{jl} < CR, \\ v_{jl}, & \text{otherwise}, \end{cases} \tag{A3}$$

   where x_{jl} is a randomly selected number that satisfies $x_{jl} = U[0, 1)$.
4. If some of parameters w_{jl} violate the constraints, they are returned into the feasible area:

$$v_{jl} = \max(\min(w_{jl}, L_j^{\max}), L_j^{\min}). \tag{A4}$$

   Then $v_{jl}, j \in [1, m], l \in [1, 3]$, is the population for the next generation.
5. If ig reaches ng or the population has little dispersion, due to $\overline{g} < tol \cdot s_g$, being $\overline{g}$ the mean and s_g the standard deviation of $g_j, j \in [1, m]$, then the iteration is halted, with the best individual as the solution. Otherwise step 1 follows.

Numerical parameters adopted in this study were: $m = 15$, $ng = 60$, $tol = 0.0025$, $F = 0.5671$, $CR = 0.5$. Weight of the best individual in the mixing, $\mu = 0.2 + 0.8\,(ig/ng)^2$, changes at every generation, ig. This enables the optimization algorithm to first widely explore the search space, but afterward it focuses on the exploitation of the most promising area. For further information on DE, the reader is referred to Chakraborty (2008) and Feoktistov (2006).

Data Availability Statement

All CTD casts and current meter data used in this work can be accessed upon request at the SeaDataNet repository (www.seadatanet.org).

Acknowledgments
The authors are very grateful to H. L. Bryden for reviewing the original manuscript and stimulating future research. Authors also appreciate the constructive comments and suggestions from two anonymous reviewers that helped to improve this manuscript. S. Piñeiro acknowledges the pre-doctoral FPI Fellowship (BES-2015-074316) support from the Spanish Ministry of Science and Innovation (MICINN), co-funded by the European Social Fund. The authors would also like to thank the fieldwork and effort made by all the personnel involved in the RADMED and ATHAPOC surveys. This work was supported by the ATHAPOC project (CTM2014-54374-R), funded by *Plan Nacional I + D + I* and by the RADMED project, funded by the *Instituto Español de Oceanografía*. Some of the instruments were made available by the Balearic Islands Coastal Observing and Forecasting System (ICTS-SOCIB), the Mediterranean Institute for Advanced Studies (IMEDEA CSIC-UIB), and the University of the Balearic Islands (UIB).

References

Benthuysen, J., & Thomas, L. N. (2012). Friction and diapycnal mixing at a slope: Boundary control of potential vorticity. *Journal of Physical Oceanography*, *42*(9), 1509–1523. https://doi.org/10.1175/JPO-D-11-0130.1

Beuvier, J., Béranger, K., Brossier, C. L., Somot, S., Sevault, F., Drillet, Y., et al. (2012). Spreading of the Western Mediterranean Deep Water after winter 2005: Time scales and deep cyclone transport. *Journal of Geophysical Research*, *117*(7), 1–26. https://doi.org/10.1029/2011JC

Bindoff, N. L., & McDougall, T. J. (1994). Diagnosing climate change and ocean ventilation using hydrographic data. *Journal of Physical Oceanography*, *24*(6), 1137–1152. https://doi.org/10.1175/1520-0485(1994)024(1137:DCCAOV)2.0.CO;2

Bryden, H. L., Schroeder, K., Borghini, M., Vetrano, A., & Sparnocchia, S. (2014). Mixing in the deep waters of the Western Mediterranean. In G. L. E. Borzelli, M. Gacic, P. Lionello, & P. Malanotte-Rizzoli (Eds.), *The Mediterranean sea: Temporal variability and spatial patterns* (pp. 51–58). Oxford: John Wiley and Sons Inc. https://doi.org/10.1002/9781118847572

Canals, M., Puig, P., Durrieu de Madron, X., Heussner, S., Palanques, A., & Fabres, J. (2006). Flushing submarine canyons. *Nature*, *444*(7117), 354–357. https://doi.org/10.1038/nature05271

Chakraborty, U. K. (2008). In U. K. Chakraborty (Ed.), Advances in differential evolution, No. November). (Vol. 143). Berlin: Springer Berlin Heidelberg. https://doi.org/10.1007/978-3-540-68830-3

Crank, J., & Nicolson, P. (1947). A practical method for numerical evaluation of solutions of partial differential equations of the heat-conduction type. *Mathematical Proceedings of the Cambridge Philosophical Society*, *43*(1), 50–67. https://doi.org/10.1017/S0305004100023197

Cuypers, Y., Bouruet-Aubertot, P., Marec, C., & Fuda, J. L. (2012). Characterization of turbulence from a fine-scale parameterization and microstructure measurements in the Mediterranean Sea during the BOUM experiment. *Biogeosciences*, *9*(8), 3131–3149. https://doi.org/10.5194/bg-9-3131-2012

Durrieu de Madron, X., Houpert, L., Puig, P., Sanchez-Vidal, A., Testor, P., Bosse, A., et al. (2013). Interaction of dense shelf water cascading and open-sea convection in the northwestern Mediterranean during winter 2012. *Geophysical Research Letters*, *40*(7), 1379–1385. https://doi.org/10.1002/grl.50331

Durrieu de Madron, X., Ramondenc, S., Berline, L., Houpert, L., Bosse, A., Martini, S., et al. (2017). Deep sediment resuspension and thick nepheloid layer generation by open-ocean convection. *Journal of Geophysical Research*, *122*, 2291–2318. https://doi.org/10.1002/2016JC012062

Durrieu De Madron, X., Zervakis, V., Theocharis, A., & Georgopoulos, D. (2005). Comments on "Cascades of dense water around the world ocean". *Progress in Oceanography*, *64*(1), 83–90. https://doi.org/10.1016/j.pocean.2004.08.004

Feoktistov, V. (2006). In: Differential evolution (Vol. 5). Boston, MA: Springer US. https://doi.org/10.1007/978-0-387-36896-2

Ferrari, R., Mashayek, A., McDougall, T. J., Nikurashin, M., & Campin, J. M. (2016). Turning ocean mixing upside down. *Journal of Physical Oceanography*, *46*(7), 2239–2261. https://doi.org/10.1175/JPO-D-15-0244.1

Ferron, B., Bouruet-Aubertot, P., Cuypers, Y., Schroeder, K., & Borghini, M. (2017). How important are diapycnal mixing and geothermal heating for the deep circulation of the Western Mediterranean?. *Geophysical Research Letters*, *44*, 7845–7854. https://doi.org/10.1002/2017GL074169

Font, J., Béranger, K., Bryden, H., Budillon, G., Fuda, J. L., Gačić, M., et al. (2009). Executive summary of CIESM workshop 38 "Dynamics of Mediterranean deep waters". In F. Briand (Ed.), Ciesm workshop monographs (Vol. 38, pp. 5–17). Monaco: CIESM.

Font, J., Puig, P., Salat, J., & Palanques, A. (2007). Sequence of hydrographic changes in NW Mediterranean deep water due to the exceptional winter of 2005. *Scientia Marina*, *71*(2), 339–346. https://doi.org/10.3989/scimar.2007.71n2339

Fuda, J. L., Bengara, L., Ismail, S. B., Curtil, C., Moumni, B. E., Font, J., et al. (2009). Recent dense water formation in the Med western basin, as observed by HYDROCHANGES. In F. Briand (Ed.), Ciesm workshop monographs (Vol. 38, pp. 29–33). Monaco: CIESM.

Houpert, L., Durrieu de Madron, X., Testor, P., Bosse, A., D'Ortenzio, F., Bouin, M. N., et al. (2016). Observations of open-ocean deep convection in the northwestern Mediterranean Sea: Seasonal and interrannual variability of mixing and deep water masses for the 2007-2013 period. *Journal of Geophysical Research: Oceans*, *121*, 8139–8171. https://doi.org/10.1002/2016JC011857

Jayne, S. R. (2009). The impact of Abyssal mixing parameterizations in an ocean general circulation model. *Journal of Physical Oceanography*, *39*(7), 1756–1775. https://doi.org/10.1175/2009JPO4085.1

Kelley, D. E. (1984). Effective diffusivities within oceanic thermohaline staircases. *Journal of Geophysical Research*, *89*(11), 484–488. https://doi.org/10.1029/JC089iC06p10484

Kelley, D. E. (1990). Fluxes through diffusive staircases: A new formulation. *Journal of Geophysical Research*, *95*(C3), 3365–3371. https://doi.org/10.1029/JC095iC03p03365

Kelley, D. E., Fernando, H. J. S., Gargett, A. E., Tanny, J., & Özsoy, E. (2003). The diffusive regime of double-diffusive convection. *Progress in Oceanography*, *56*(3–4), 461–481. https://doi.org/10.1016/S0079-6611(03)00026-0

Klymak, J., & Nash, J. D. (2009). Estimates of mixing. In H. J. Steele, S. A. Thorpe, & K. K. Turekian (Eds.), Encyclopedia of ocean sciences. (2nd ed., Vol. 2, pp. 288–298). London: Elsevier Ltd. https://doi.org/10.1016/B978-012374473-9.00615-9

López-Jurado, J. L., Balbín, R., Alemany, F., Amengual, B., Aparicio-González, A., Fernandez de Puelles, M. L., et al. (2015). The RADMED monitoring programme as a tool for MSFD implementation: Towards an ecosystem-based approach. *Ocean Science*, *11*, 897–908. https://doi.org/10.5194/os-11-897-2015

López-Jurado, J. L., González-Pola, C., & Vélez-Belchí, P. (2005). Observation of an abrupt disruption of the long-term warming trend at the Balearic Sea, western Mediterranean Sea, in summer 2005. *Geophysical Research Letters*, *32*(24), 1–4. https://doi.org/10.1029/2005GL024430

Lueck, R. (2001). Turbulence in the benthic boundary layer. In J. H. Steele, S. A. Thorpe, & K. K. Turekian (Eds.), *Elements of physical oceanography*. (2nd ed., pp. 311–316). London: Elsevier.

Marshall, J., & Schott, F. (1999). Open-ocean convection: Observations, theory and models. *Reviews of Geophysics*, *37*(98), 1–64. https://doi.org/10.1029/98RG02739

MEDOC Group. (1970). Observation of formation of deep water in the Mediterranean Sea. *Nature*, *227*, 1037–1040.

Naveira-Garabato, A. C., Frajka-Williams, E. E., Spingys, C. P., Legg, S., Polzin, K. L., Forryan, A., et al. (2019). Rapid mixing and exchange of deep-ocean waters in an abyssal boundary current. *Proceedings of the National Academy of Sciences*, *116*(27), 13233–13238. https://doi.org/10.1073/pnas.1904087116

Piñeiro, S., González-Pola, C., Fernández-Díaz, J. M., & Balbin, R. (2019). Thermohaline evolution of the Western Mediterranean Deep Waters Since 2005: Diffusive stages and interannual renewal injections. *Journal of Geophysical Research: Oceans*, *124*(12), 8747–8766. https://doi.org/10.1029/2019JC015094

Puig, P., Durrieu de Madron, X., Salat, J., Schroeder, K., Martín, J., Karageorgis, A. P., et al. (2013). Thick bottom nepheloid layers in the western Mediterranean generated by deep dense shelf water cascading. *Progress in Oceanography*, *111*, 1–23. https://doi.org/10.1016/j.pocean.2012.10.003

Puig, P., Palanques, A., Font, J., Salat, J., Latasa, M., & Scharek, R. (2009). Interactions between open-sea convection and shelf cascading dense waters in the formation of the Western Mediterranean Deep Water. In F. Briand (Ed.), Ciesm workshop monographs. (Vol. 38, pp. 81–89). Monaco: CIESM.

Radko, T. (2013). *Double-diffusive convection* (1st ed.). New York: Cambridge University Press.

Ruddick, B. (1983). A practical indicator of the stability of the water column to double-diffusive activity. *Deep Sea Research A, Oceanographic Research Papers*, *30*(10), 1105–1107. https://doi.org/10.1016/0198-0149(83)90063-8

Salat, J., Emelianov, M., & López-Jurado, J. L. (2006). Unusual extension of Western Mediterranean deep water formation during winter 2005. *5ª asamblea hispano-portuguesa de geodesia y geofisica* (pp. 1–4). Seville.

Salat, J., Puig, P., & Latasa, M. (2010). Violent storms within the Sea: Dense water formation episodes in the NW Mediterranean. *Advances in Geosciences*, *26*, 53–59. https://doi.org/10.5194/adgeo-26-53-2010

Schmitt, R. W. (1981). Form of the temperature-salinity relationship in the central water: Evidence for double-diffusive mixing. *Journal of Physical Oceanography*, *11*(7), 1015–1026. https://doi.org/10.1175/1520-0485(1981)011⟨1015:FOTTSR⟩2.0.CO;2

Schmitt, R. W. (2009). Double-diffusive convection. In H. J. Steele, S. A. Thorpe, & K. K. Turekian (Eds.), Encyclopedia of ocean sciences. (2nd ed., Vol. 2, pp. 162–170). London: Elsevier Ltd.

Schroeder, K., Chiggiato, J., Bryden, H. L., Borghini, M., & Ismail, S. B. (2016). Abrupt climate shift in the Western Mediterranean Sea. *Nature Scientific Reports*, *6*, 1–7. https://doi.org/10.1038/srep23009

Schroeder, K., Gasparini, G. P., Tangherlini, M., & Astraldi, M. (2006). Deep and intermediate water in the western Mediterranean under the influence of the Eastern Mediterranean Transient. *Geophysical Research Letters*, *33*(21), 2–7. https://doi.org/10.1029/2006GL027121

Schroeder, K., Millot, C., Bengara, L., Ben Ismail, S., Bensi, M., Borghini, M., et al. (2013). Long-term monitoring programme of the hydrological variability in the Mediterranean Sea: A first overview of the HYDROCHANGES network. *Ocean Science*, *9*(2), 301–324. https://doi.org/10.5194/os-9-301-2013

Schroeder, K., Ribotti, A., Borghini, M., Sorgente, R., Perilli, A., & Gasparini, G. P. (2008). An extensive western Mediterranean deep water renewal between 2004 and 2006. *Geophysical Research Letters*, *35*(18), L18605. https://doi.org/10.1029/2008GL035146

Send, U., Font, J., & Mertens, C. (1996). Recent observation indicates convection's role in deep water circulation. *EOS Transactions AGU*, *77*(7), 61–65. https://doi.org/10.1029/96EO00040

Send, U., & Testor, P. (2017). Direct observations reveal the deep circulation of the Western Mediterranean Sea. *Journal of Geophysical Research: Oceans*, *122*(12), 10091–10098. https://doi.org/10.1002/2016JC012679

Smith, R. O., Bryden, H. L., & Stansfield, K. (2008). Observations of new western Mediterranean deep water formation using Argo floats 2004-2006. *Ocean Sciences*, *4*, 133–149. https://doi.org/10.5194/os-4-133-2008

Somot, S., Houpert, L., Sevault, F., Testor, P., Bosse, A., Taupier-Letage, I., et al. (2018). Characterizing, modelling and understanding the climate variability of the deep water formation in the North-Western Mediterranean Sea. *Climate Dynamics*, *51*(3), 1179–1210. https://doi.org/10.1007/s00382-016-3295-0

Testor, P., & Gascard, J. C. (2003). Large-scale spreading of deep waters in the Western Mediterranean Sea by submesoscale coherent eddies. *Journal of Physical Oceanography*, *33*(1), 75–87. https://doi.org/10.1175/1520-0485(2003)033⟨0075:LSSODW⟩2.0.CO;2

Testor, P., & Gascard, J. C. (2006). Post-convection spreading phase in the Northwestern Mediterranean Sea. *Deep-Sea Research I: Oceanographic Research Papers*, *53*(5), 869–893. https://doi.org/10.1016/j.dsr.2006.02.004

Waterhouse, A. F., MacKinnon, J. A., Nash, J. D., Alford, M. H., Kunze, E., Simmons, H. L., et al. (2014). Global patterns of diapycnal mixing from measurements of the turbulent dissipation rate. *Journal of Physical Oceanography*, *44*(7), 1854–1872. https://doi.org/10.1175/JPO-D-13-0104.1

Zhang, J., & Schmitt, R. W. (2000). The impact of salt fingering on the thermohaline circulation under mixed boundary conditions. *Journal of Physical Oceanography*, *30*(6), 1223–1231. https://doi.org/10.1175/1520-0485(2000)030⟨1223:TIOSFO⟩2.0.CO;2

Zhang, J., Schmitt, R. W., & Huang, R. X. (1998). Sensitivity of the GFDL modular ocean model to parameterization of double-diffusive processes. *Journal of Physical Oceanography*, *28*(4), 589–605. https://doi.org/10.1175/1520-0485(1998)028⟨0589:SOTGMO⟩2.0.CO;2